

Heterometallic trinuclear 3d–4f–3d compounds based on a hexadentate Schiff base ligand



Beata Cristóvão ^{a,*}, Julia Kłak ^b, Robert Pełka ^c, Barbara Miroslaw ^d, Zbigniew Hnatejko ^e

^a Department of General and Coordination Chemistry, Maria Curie-Sklodowska University, Maria Curie-Sklodowska sq. 2, 20-031 Lublin, Poland

^b Faculty of Chemistry, University of Wrocław, F. Joliot Curie 14, 50-383 Wrocław, Poland

^c Institute of Nuclear Physics, Polish Academy of Sciences, Radzikowskiego 152, 31-342 Kraków, Poland

^d Department of Crystallography, Maria Curie-Sklodowska University, Maria Curie-Sklodowska sq. 3, 20-031 Lublin, Poland

^e Faculty of Chemistry, Adam Mickiewicz University, Grunwaldzka 6, 60-780 Poznań, Poland

ARTICLE INFO

Article history:

Received 10 June 2013

Accepted 15 October 2013

Available online 26 October 2013

Keywords:

3d–4f Compound

Schiff base

Magnetism

Lanthanides

Luminescence

ABSTRACT

The new heterometallic trinuclear complexes $[Ni_2Ln(L)_2(CH_3COO)_2(MeOH)_2]NO_3 \cdot 4H_2O$ (where $Ln = Ce(III)$ **1**, $Pr(III)$ **2** and H_2L = the Schiff base resulting from the condensation of 5-bromo-3-methoxysalicylaldehyde and 1,3-diaminopropane) were synthesized and characterized by elemental analysis, FTIR, TG/DSC, TG-FTIR, single crystal X-ray diffraction, magnetic, UV-Vis and luminescence studies. In the isostructural crystals of **1** and **2** the nickel(II) and lanthanide(III) ions are bridged by two Schiff base's phenolato oxygens and additionally by the acetate ions. The clathrate type of crystal architecture in reported complexes, results in their quite high stability in air and nitrogen atmospheres at room temperature despite the relatively large amount of non-coordinated water. The temperature dependence (1.8–300 K) of the magnetic susceptibility investigations and the field-dependent magnetization indicate crystal field effect, as well as, the presence of an antiferromagnetic interaction between spin carriers of Ni^{II} and Ln^{III} pairs in the $Ni^{II}-Ce^{III}-Ni^{II}$ (**1**) and $Ni^{II}-Pr^{III}-Ni^{II}$ (**2**) compounds operating via oxygen atoms ($J_{NiCe} = -1.1(4) \text{ cm}^{-1}$ (**1**) and $J_{NiPr} = -1.3(8) \text{ cm}^{-1}$ (**2**)).

© 2013 Elsevier Ltd. All rights reserved.

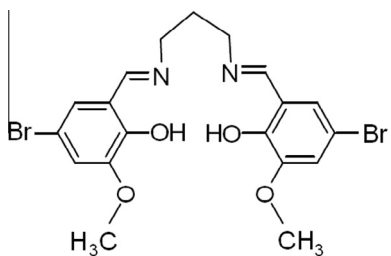
1. Introduction

In recent years, there is growing interest in the synthesis, structure and physicochemical properties of heteronuclear compounds consisted of simultaneously 3d and 4f metal centers due to the variety of potential applications of these complexes mainly in bio-inorganic chemistry, magnetochemistry, separation processes, luminescence, environmental chemistry, electrochemistry and catalysis [1,2]. The salen-like hexadentate Schiff base derived from 5-bromo-3-methoxysalicylaldehyde and 1,3-diaminopropane (Scheme 1) contains a tetradeятate inner core formed of two imino nitrogen and two μ -phenoxo oxygen atoms and outer coordination compartment that chelates through two μ -phenoxo and two methoxy oxygen atoms. The methoxy groups from the ligands derived from o-vanillin play an active role in holding rare earth cations within heterometallic complexes. This ligand is particular for 3d/4f chemistry because it is able to coordinate 3d and 4f metal ions via N and O atoms in a different way. Lanthanide ions behave as hard acids and they prefer oxygen to nitrogen donors, while 3d metal ions can coordinate to both N and O donors [3,4]. In contrast to the number reports concerning the synthesis and magnetic

behavior of 3d–4f heteronuclear compounds from Schiff base ligands [1,3–11], there are relatively less reports on their thermal and photophysical properties [1–3,12–15]. The results of thermal analysis allowed us to confirm the presence of lattice and/or coordination water molecules in the crystal structure of complexes and to determine the endothermic and/or exothermic effects connected with processes such as: desolvation, dehydration, melting and decomposition. The near-infrared and photoluminescence (PL) properties of lanthanide(III) (Pr^{3+} , Nd^{3+} , Eu^{3+} , Tb^{3+} , Er^{3+} , Yb^{3+}) complexes have been of special interest in recent years because these ions exhibit long luminescent lifetime, large Stoke's shifts and characteristic line-like emission bands. The luminescence properties of homo- (4f) and heterometallic (3d–4f) complexes with "salen" style Schiff base ligands were studied by Jones et al. [2,3,12–15] and they indicated that the photophysical properties of lanthanide ions depend markedly on the environment surrounding the metal center. Solvents containing O–H groups (i.e. H_2O and CH_3OH) can efficiently quench the luminescence of lanthanide ions. However, if the O–H fragment is replaced by O–D, this process becomes much less efficient. As a continuation of our investigation on 3d–4f multinuclear coordination compounds with *N,N'*-bis (5-bromo-3-methoxysalicylidene)propylene-1,3-diamine in this paper we describe the results of spectral, magnetic, thermal, luminescence (in the case of **2**) studies and crystal structures of new

* Corresponding author.

E-mail address: beata.cristovao@poczta.umcs.lublin.pl (B. Cristóvão).

**Scheme 1.** Schiff base ligand H₂L.

heteronuclear [Ni₂Ce(L)₂(CH₃COO)₂(MeOH)₂]NO₃·4H₂O (**1**) and [Ni₂Pr(L)₂(CH₃COO)₂(MeOH)₂]NO₃·4H₂O (**2**) complexes.

2. Experimental

2.1. Materials

The reagents and solvents i.e. Ni(CH₃COO)₂·4H₂O, Ce(NO₃)₃·6H₂O, Pr(NO₃)₃·6H₂O, 1,3-diaminopropane, 5-bromo-2-hydroxy-3-methoxybenzaldehyde and methanol used for synthesis were commercially available from Aldrich Chemical Company and Polish Chemical Reagents. They were used as received without further purification.

2.2. Synthesis

2.2.1. N,N'-bis(5-bromo-3-methoxysalicylidene)propylene-1,3-diamine, H₂L

The synthesis of the Schiff base (N,N'-bis(5-bromo-3-methoxysalicylidene)propylene-1,3-diamine, C₁₉H₂₀Br₂N₂O₄) abbreviated as H₂L was described earlier [4].

2.2.2. [Ni₂Ce(L)₂(CH₃COO)₂(MeOH)₂]NO₃·4H₂O (**1**)

To a stirred solution of the Schiff base H₂L (0.4 mmol, 0.1999 g) in hot methanol (30 mL) was added Ni(CH₃COO)₂·4H₂O (0.4 mmol, 0.0995 g) in hot MeOH (10 mL). As a result the brown solid appeared. The obtained mixture was vigorously stirred for about 30 min, after this time the solution of Ce(NO₃)₃·6H₂O (0.2 mmol, 0.0868 g) in MeOH (5 mL) was added. Upon addition of lanthanide nitrate the brown precipitate dissolved and the solution became pale-green. The resulting solution was left to stir for about 30 min, during which time it did not change the color. Then the solution was clarified by filtration and allowed to stand at low temperature. Pale-green crystals were formed during three weeks. Yield: 34%. Anal. Calc. (1570.13): C, 33.66; H, 3.69; N, 4.46; Ni, 7.48; Ce, 8.92. Found: C, 33.12; H, 3.20; N, 4.80; Ni, 7.30; Ce, 8.70%. FTIR bands (KBr, cm⁻¹): 3420m, 2932w, 2846w 1644s, 1570w, 1468s, 1440m, 1384s, 1292s, 1236s, 1214m, 1104w, 1012w, 966w, 852w, 780m, 760w, 692w, 628w, 576w, 544w, 462m.

2.2.3. [Ni₂Pr(L)₂(CH₃COO)₂(MeOH)₂]NO₃·4H₂O (**2**)

Complex **2** was synthesized according to the procedure followed for **1** (Pr(NO₃)₃·6H₂O, 0.2 mmol, 0.0870 g). Yield: 36%. Anal. Calc. (1570.92): C, 33.64; H, 3.69; N, 4.46; Ni, 7.47; Pr, 8.97. Found: C, 33.25; H, 3.15; N, 4.65; Ni, 7.12; Pr, 8.49%. FTIR bands (KBr, cm⁻¹): 3424m, 2932 w, 2848 w 1640s, 1572w, 1468s, 1440m, 1384s, 1292s, 1236s, 1216m, 1100 w, 1012w, 966w, 852w, 780m, 760w, 692w, 628w, 578w, 540w, 460m.

2.3. Methods

The contents of carbon, hydrogen and nitrogen in the analysed compounds were determined by elemental analysis using a CHN

2400 Perkin Elmer analyser. The contents of nickel and lanthanides were established using ED XRF spectrophotometer (Canberra-Packard).

The FTIR spectra of complexes were recorded over the range of 4000–400 cm⁻¹ using M-80 spectrophotometer (Carl Zeiss Jena). Samples for FTIR spectra measurements were prepared as KBr discs. The magnetization of the **1** and **2** powdered samples was measured over the temperature range 1.8–300 K using a Quantum Design SQUID – based MPMSXL-5 type magnetometer. The superconducting magnet was generally operated at a field strength ranging from 0 to 5 T. Measurements sample of compounds were made at magnetic field 0.5 T. The SQUID magnetometer was calibrated with the palladium rod sample. Corrections are based on subtracting the sample – holder signal and contribution χ_D estimated from the Pascal's constants [16]. The UV–Vis spectra of Schiff base ligand and compounds (methanol solution 2 × 10⁻⁵ M) were recorded in 10 × 10 mm quartz cells over the range 200–900 nm using GENESYS 10S UV–Vis spectrophotometer. Emission spectra of the free Schiff base ligand H₂L and complexes were recorded at concentrations of 2.5 × 10⁻⁵ M in methanol at room temperature. Excitation and emission spectra were measured on a Hitachi 7000 spectrofluorimeter with excitation and emission slits of 5 nm. The emission quantum yield for mononuclear Ni(II) complex was measured using a relative method with anthracene as the standard [17] and calculated from the equation [18].

$$\phi = \frac{I_x A_s n_x^2}{I_s A_x n_s^2}$$

where: ϕ is the quantum yield, subscript s stands for the reference and x for the sample. A is the absorbance at the excitation wavelength, n is the refractive index and I is the integrated emission intensity. Thermal analyses of the prepared compounds were carried out by the thermogravimetric (TG) and differential scanning calorimetry (DSC) methods using the SETSYS 16/18 analyser (Setaram). The experiments were carried out under air flow in the temperature range of 20–1000 °C at a heating rate of 10 °C min⁻¹. The samples (7.38 mg (**1**) and 7.85 mg (**2**)) were heated in Al₂O₃ crucibles.

The X-ray powder diffraction patterns of the products of decomposition process were taken on a HZG-4 (Carl-Zeiss, Jena) diffractometer using Ni filtered Cu K α radiation. The measurements were made within the range of 2θ = 4–80° by means of Bragg–Brentano method. The TG–FTIR coupled measurements have been carried out using a Netzsch TG apparatus coupled with a Bruker FTIR IFS66 spectrophotometer. The samples of about 10 mg were heated up to 800 °C (compounds) and 900 °C (Schiff base), respectively at a heating rate of 10 °C min⁻¹ in flowing argon atmosphere.

2.4. X-ray crystal structure determination

Intensity measurements were carried out at 295 K with Oxford Diffraction Xcalibur CCD diffractometer with the graphite-monochromatized MoK α radiation ($\lambda = 0.71073$ Å). Data sets were collected using the ω scan technique, with an angular scan width of 1.0°. The programs CrysAlis CCD and CrysAlis Red [19] were used for data collection, cell refinement and data reduction. Analytical absorption correction based on the indexing of crystal faces was applied [20]. The structures were solved by direct methods using SHELXS-97 and refined by the full-matrix least-squares on F² using the SHELXL-97 [21]. The lanthanide ions in **1** and **2** lie on the center of inversion with sof = 0.5. The nitrate ion is disordered over two positions by the center of inversion (sof's = 0.5). Because of disorder in nitrate molecule the bond length restraints were applied by DFIX instructions to 1.23(1) and 2.13(1) Å for N–O and O–O

distances, respectively. Non-hydrogen atoms with the exception of disordered nitrate N and O atoms and one water molecule in **1** and **2** were refined with anisotropic displacement parameters. The C-bound H atoms were positioned geometrically and the ‘riding’ model for the C-H bonds was used in the refinement with $U_{\text{iso}}(\text{H}) = 1.2 U_{\text{eq}}(\text{C})$ or $=1.5 U_{\text{eq}}(\text{C})$ for methyl H atoms. The O-bound H atoms were located in a difference Fourier maps and refined using a riding model with O-H distances of 0.82–0.85 Å and $U_{\text{iso}}(\text{H}) = 1.5 U_{\text{eq}}(\text{O})$. The summary of experimental details and the crystal structure refinement parameters are given in Table 1. The molecular plots were drawn with ORTEP3 for Windows [22] and Diamond [23].

3. Results and discussion

3.1. Structural description

The two isostructural heterometallic trinuclear Schiff base complexes $[\text{Ni}_2\text{Ln}(\text{L})_2(\text{CH}_3\text{COO})_2(\text{MeOH})_2]\text{NO}_3 \cdot 4\text{H}_2\text{O}$ (where $\text{Ln} = \text{Ce}^{\text{III}}$ (**1**) and Pr^{III} (**2**) and $\text{L} = \text{C}_{19}\text{H}_{18}\text{N}_2\text{O}_4\text{Br}_2 = \text{N,N}'\text{-bis}(5\text{-bromo-3-methoxysalicylidene)-1,3-diaminopropanoato}$) crystallize in the $P2_1/n$ space group. The atom numbering scheme of **1** is shown in Fig. 1 (analogues for the compound **2**). The selected bond lengths and angles are given in Table 2. In these compounds rare earth(III) ion occupies the center of inversion coordinating ten oxygen atoms (eight O atoms from two hexadentate Schiff base ligands and two O atoms – both coming from two acetate ions acting as bidentate bridging ligands) which form pentagonal antiprism (Figs. 1 and 2). The nickel(II) ions are hexacoordinated. They are located in the inner N_2O_2 cavities of the two bicompartimental Schiff base ligands and their coordination polyhedra adopt a distorted octahedral geometry (Figs. 1 and 2). The oxygen atoms of methanol molecules and acetate anions (bridging to Ln^{III}) occupy the axial sites. The Ni^{II} ions lie in the mean $\text{N}1\text{N}2\text{O}1\text{O}2$ plane of the Schiff base ligand with deviation being only 0.034 and 0.039 Å for **1** and **2**, respectively. As shown in Figs. 1 and 2 each pair of the $\text{Ni}(\text{II})$ and $\text{Ln}(\text{III})$ metal ions are linked by two bridging phenoxy oxygen atoms ($\text{O}1$ and $\text{O}2$) of the Schiff base ligand and additionally one bidentate bridging carboxylate group ($\text{O}6\text{C}20\text{O}7$) of the acetate ion. In both **1** and **2**, the average distances for the M-O bonds are significantly different ($\text{Ni}-\text{O}$ ca. 2.0 Å, and $\text{Ce}/\text{Pr}-\text{O}$ ca. 2.5–2.9 Å). The $\text{Ln}1-\text{O}$ bond lengths

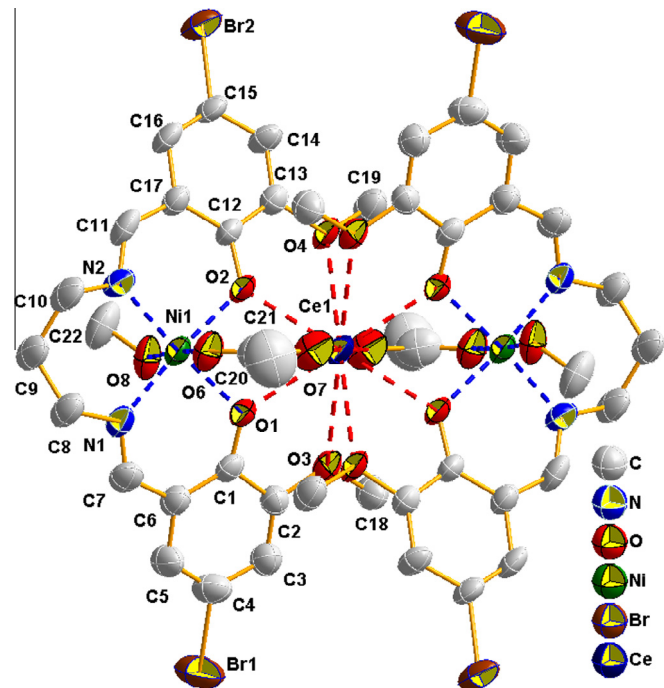


Fig. 1. Molecular structure and atom numbering scheme of $\text{Ni}^{\text{II}}\text{-Ce}^{\text{III}}\text{-Ni}^{\text{II}}$ (**1**) at 20% probability, hydrogen atoms, nitrate ion and water molecules in the outer coordination sphere are omitted for clarity. Molecule lies on the center of inversion thus only half of the molecule is symmetrically independent and was numbered in the picture, symmetry code $i: -x, -y, -z$.

depend on the nature of the oxygen atoms and increase in sequence acetate < phenolato < methoxo (Table 2). Such differences in bond distance are expected due to their differences in ionic size of 3d and 4f metal ions and are observed in related 3d–4f compounds [4,7,5]. The dihedral angles (α) between the ($\text{O}1\text{Ni}1\text{O}2$) and ($\text{O}1\text{Ce}1/\text{Pr}1\text{O}2$) planes are 24.7° (**1**) and 25.8° (**2**), respectively (Table 2). The intramolecular separations $\text{Ni}1\cdots\text{Ce}/\text{Pr}$, and $\text{Ni}1\cdots\text{Ni}1^i$ (symmetry code (i) $-x, -y, -z$) are ca. 3.5 and 7.1 Å, respectively (Table 2) agree with the observed ranges of values

Table 1
Crystallographic data for crystals **1** and **2**.

	1	2
Empirical formula	$\text{C}_{44}\text{H}_{58}\text{Br}_4\text{N}_5\text{O}_{21}\text{Ni}_2\text{Ce}$	$\text{C}_{44}\text{H}_{58}\text{Br}_4\text{N}_5\text{O}_{21}\text{Ni}_2\text{Pr}$
Formula weight	1570.13	1570.92
T (K)	295(2)	295(2)
Crystal system	monoclinic	monoclinic
Space group	$P2_1/n$	$P2_1/n$
a (Å)	13.815(1)	13.858(2)
b (Å)	15.667(1)	15.654(1)
c (Å)	14.885(1)	14.844(2)
β (°)	117.06(1)	116.98(2)
V (Å ³)	2869.0(4)	2872.0(8)
Z; Z'	2; 0.5	2; 0.5
Crystal form/colour	plate/green	block/green
Crystal size (mm)	0.40 × 0.20 × 0.08	0.40 × 0.40 × 0.38
D _{calc} (g cm ⁻³)	1.818	1.816
μ (mm ⁻¹)	4.292	4.342
Absorption correction	analytical	analytical
θ (°)	3.02–25.24	3.01–25.24
Reflections collected/unique (R_{int})	10987/5136 (0.0513)	10882/5078 (0.0314)
Data/restraints/parameters	5136/7/342	5078/7/342
Goodness-of-fit (GOF) on F^2	1.004	1.035
R_1 , wR_2 [$I > 2\sigma(I)$]	0.0589, 0.1425	0.0519, 0.1292
R_1 , wR_2 (all data)	0.1026, 0.1708	0.0719, 0.1448
$\Delta\rho_{\text{max}}, \Delta\rho_{\text{min}}$ (e Å ⁻³)	0.964, -0.750	0.971, -0.753

Table 2

Selected geometric parameters (\AA , $^\circ$) in the coordination environments of metal centers.

	1	2
Bond lengths		
Ln1–O1	2.507(5)	2.476(4)
Ln1–O2	2.492(5)	2.462(4)
Ln1–O3	2.900(5)	2.904(5)
Ln1–O4	2.931(5)	2.933(4)
Ln1–O7	2.434(6)	2.414(6)
Ni1–N1	2.037(6)	2.043(5)
Ni1–N2	2.014(6)	2.024(6)
Ni1–O1	2.036(5)	2.027(4)
Ni1–O2	2.062(5)	2.041(4)
Ni1–O6	2.059(6)	2.065(5)
Ni1–O8	2.170(6)	2.179(5)
Ni1–Ln1	3.570(1)	3.538(1)
Ni1···Ni1 ⁱ	7.141(2)	7.076(2)
symmetry code: ⁱ $-x, -y, -z$		
Bond angles		
Ni1–O1–Ln1	103.1(2)	103.1(2)
Ni1–O2–Ln1	102.9(2)	103.2(2)
O1–Ln1–O2	65.1(2)	64.9(1)
N2–Ni1–N1	95.6(3)	96.3(2)
N2–Ni1–O1	173.6(2)	172.8(2)
N2–Ni1–O2	91.7(2)	91.7(2)
N1–Ni1–O2	172.2(2)	171.2(2)
O1–Ni1–N1	90.5(2)	90.7(2)
O1–Ni1–O2	82.0(2)	81.3(1)
O1–Ni1–O6	94.0(2)	94.0(2)
O2–Ni1–O6	95.5(2)	95.6(2)
N1–Ni1–O6	87.2(2)	87.4(2)
N2–Ni1–O6	88.0(3)	88.3(2)
N1–Ni1–O8	90.6(2)	90.1(2)
N2–Ni1–O8	95.4(2)	95.6(2)
O1–Ni1–O8	82.8(2)	82.4(2)
O2–Ni1–O8	86.3(1)	86.4(1)
O6–Ni1–O8	176.1(2)	175.6(2)
O1–Ln1–O3	56.9(2)	57.2(1)
O2–Ln1–O3	112.1(2)	112.1(1)
O7–Ln1–O3	116.6(2)	117.2(2)
O1–Ln1–O4	112.9(2)	112.9(1)
O2–Ln1–O4	56.7(1)	57.0(1)
O3–Ln1–O4	119.6(2)	119.1(1)
O7–Ln1–O1	77.5(2)	78.5(2)
O7–Ln1–O2	78.9(2)	79.7(2)
O7–Ln1–O4	117.6(2)	118.0(2)
α	24.7(2)	25.8(2)

α – dihedral angle between the Ni1O1O2 and Ln1O1O2 planes.

for polynuclear Ni^{II}–Ln^{III} complexes [4,7,5]. Intermolecular M···M separations in the Ni^{II}–Ln^{III}–Ni^{II} structures indicate well separation of the trinuclear 3d–4f–3d cores. Because of the special position of the molecule in the unit cell two Ni^{II} and one Ln^{III} ions are arranged in a line, with a Ni1–Ln1–Ni1ⁱ (symmetry code (*i*): $-x, -y, -z$) angle equal to 180°. Crystals of **1** and **2** are molecular structure with non-coordinated water molecules and nitrate ions occupying the cages in the crystal net formed by the molecules of trinuclear complexes (Fig. 3). Inside these cavities they are involved in extensive network of hydrogen bonds (Table 3). It is worth noticing, that the space inside each cage is large enough to enable some disorder of the guest molecules, but the crystal structure of the host molecules is dense enough to make the crystals air stable.

3.2. Thermal analysis

The thermal behavior of heterometallic trinuclear compounds [Ni₂Ln(L)₂(CH₃COO)₂(MeOH)₂]NO₃·4H₂O (where Ln = Ce^{III} (**1**) and Pr^{III} (**2**) and L = C₁₉H₁₈N₂O₄Br₂) were investigated in air and argon atmosphere (Figs. 4 and 5). The isostructural complexes are stable at room temperature and their decomposition processes proceed in

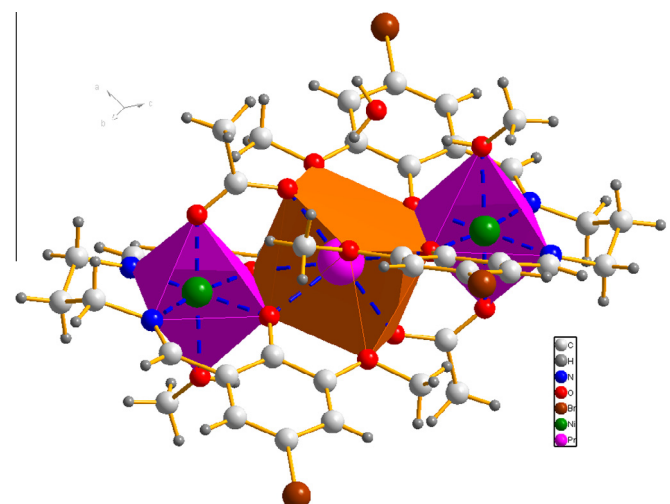


Fig. 2. The coordination environment of cations in **2**.

the similar way. Heating the samples up to ca. 190 °C in air atmosphere leads to the weight loss of 7.80% (calculated 8.66%) (**1**) and 7.60% (calculated 8.66%) (**2**) consistent with the lose simultaneously four lattice water molecules and two coordinated molecules of methanol. This process is accompanied with endothermic effect seen on the DSC curves. As the temperature is increased the recorded TG curves exhibit mass loss in a wide temperature range 220–490 °C (**1**) 220–840 °C (**2**) which are accompanied with exothermic peaks seen on DSC curves. That may be due to the decomposition of the Schiff base ligand molecules. The decomposition process of Ni^{II}–Ln^{III}–Ni^{II} compounds is intricate and it is very difficult to distinguish intermediate solid products. The residual mixed metal oxides NiO and CeO₂ (**1**) and NiO and Pr₆O₁₁ (**2**), respectively percentages (21.22% (**1**), 20.35% (**2**)) calculated from TG curves were coincided fairly with the theoretical values (20.47% (**1**), 19.51% (**2**)). The final products were experimentally verified on the basis on their X-ray diffraction powder patterns. The synthesized compounds are more stable in argon atmosphere. As shown in Fig. 5 during heating in argon the first change in mass (4.67% (**1**) and 4.70% (**2**)) estimated from TG curves coincided fairly with the theoretical values recorded for **1** and **2** corresponds to the loss of four water molecules acting as solvent. The dehydration process has been also confirmed by the TG-FTIR analysis. The recorded FTIR spectrum (Fig. 6) at 102 °C shows characteristic bands in the wavenumber ranges 4000–3400 cm⁻¹ and 2060–1260 cm⁻¹ corresponding to stretching and deforming vibrations of H₂O molecules, respectively [24,25]. During further heating the main volatiles emitted around 230 °C (the maximum point of the DTG curve, Fig. 5) are identified generally as aromatic and aliphatic compounds and nitric oxides. The recorded TG-FTIR spectra at around 335 °C (the maximum point of the DTG curve, Fig. 5) show the characteristic doublet bands at 2240–2400 cm⁻¹ and 669 cm⁻¹, respectively assigned to stretching and deformation vibrations of carbon dioxide molecules, characteristic bands in the wavenumber ranges 4000–3400 cm⁻¹ and 2060–1260 cm⁻¹ corresponding to stretching and deforming vibrations of H₂O molecules, respectively, the bands at 2060–2240 cm⁻¹ characteristic for CO molecules and the bands indicating the presence of CH₃Br [25].

3.3. Magnetic properties

The magnetic properties of the heterotrinuclear complexes Ni^{II}–Ce^{III}–Ni^{II} (**1**) and Ni^{II}–Pr^{III}–Ni^{II} (**2**) were determined over the temperature range of 1.8–300 K. Figs. 7 and 8 show the plots of the molar magnetic susceptibility in the form of the χT product

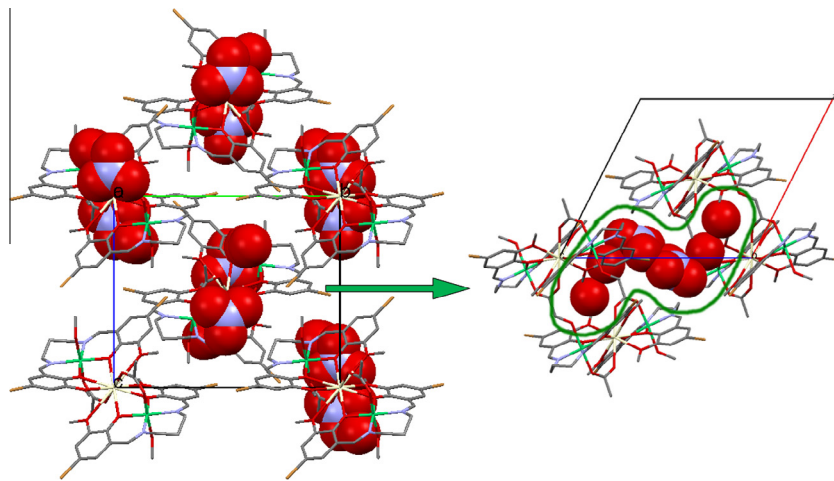


Fig. 3. The cages occupied by non-coordinated nitrate ions and water molecules (presented as van der Waals spheres) in the structure of **1**.

Table 3
Hydrogen bond parameters (\AA , $^\circ$) in **1** and **2**.

D-H...A	D-H	H...A	D-A	$\angle\text{DHA}$
1				
O5-H5A...O12	0.85	2.04	2.84(1)	156(2)
O5-H5B...O7 ⁱ	0.85	2.05	2.86(1)	161(1)
O8-H8...O5	0.85	1.96	2.79(2)	167(1)
O12-H12B...O9 ⁱⁱ	0.85	2.19	3.03(1)	166(3)
2				
O5-H5A...O12	0.85	2.04	2.84(5)	156(2)
O5-H5B...O7 ⁱ	0.85	2.05	2.86(2)	161(1)
O8-H8...O5	0.85	1.96	2.79(2)	167(1)
O12-H12B...O9 ⁱⁱ	0.85	2.19	3.03(1)	166(3)

Symmetry codes: ⁱ -x, -y, -z; ⁱⁱ x + 1, y, z.

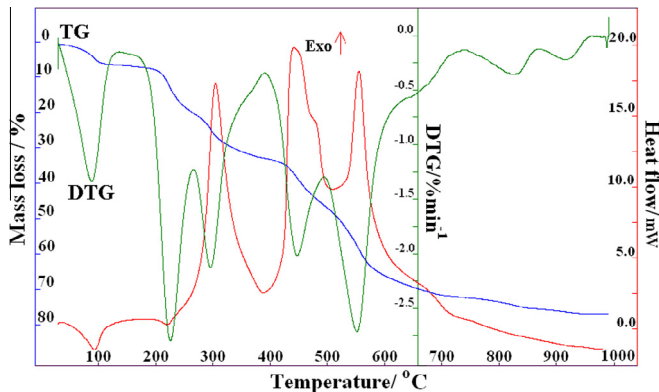


Fig. 4. TG, DTG and DSC curve of **2** in air atmosphere.

against temperature T for the powder samples of **1** and **2** (open squares). In the case of $\text{Ni}^{\text{II}}\text{-Ce}^{\text{III}}\text{-Ni}^{\text{II}}$ (**1**) the corresponding curve displays an abrupt increase in the temperature range 1.8–18 K from the value of $1.28 \text{ cm}^3 \text{ K mol}^{-1}$ to the value of $2.77 \text{ cm}^3 \text{ K mol}^{-1}$, next it almost linearly increases reaching the value of $3.18 \text{ cm}^3 \text{ K mol}^{-1}$ at 300 K which is slightly lower than that of $3.23 \text{ cm}^3 \text{ K mol}^{-1}$ comprising the free-ion contributions from two Ni^{II} ions ($S_{\text{Ni}} = 1$, $g_{\text{Ni}} = 2.2$) and one Ce^{III} ion ($J = 5/2$, $g_J = 6/7$). Similarly is for $\text{Ni}^{\text{II}}\text{-Pr}^{\text{III}}\text{-Ni}^{\text{II}}$ (**2**), the recorded curve χT versus T also shows an abrupt increase in the temperature range 1.8–12 K from the value of $0.90 \text{ cm}^3 \text{ K mol}^{-1}$ to the value of $2.41 \text{ cm}^3 \text{ K mol}^{-1}$, respectively and next it displays a more gradual increase reaching

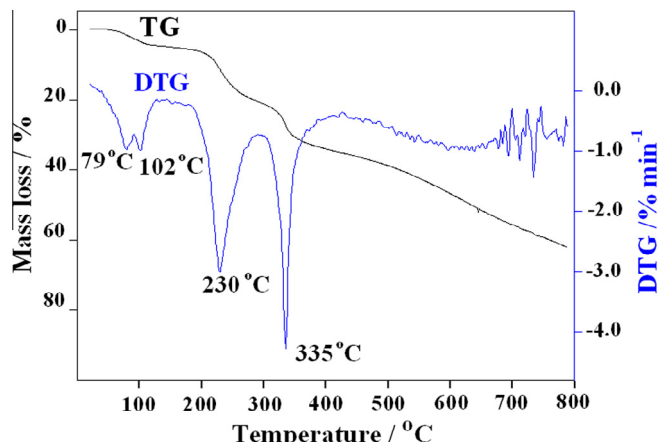


Fig. 5. TG, DTG and DSC curve of **2** in argon atmosphere.

the value of $3.75 \text{ cm}^3 \text{ K mol}^{-1}$ at 300 K which is slightly lower than that of $3.91 \text{ cm}^3 \text{ K mol}^{-1}$ comprising the free-ion contributions from two Ni^{II} ions ($S_{\text{Ni}} = 1$, $g_{\text{Ni}} = 2.15$) and one Pr^{III} ion ($J = 4$, $g_J = 4/5$). As a general trend, for the complexes of the paramagnetic Ln^{III} ions of the first half of the series the χT versus T curves are characterized by a continuous decrease as the temperature is lowered. Our results are consistent with the empirical studies concerning heterometallic $\text{Ni}^{\text{II}}\text{-4f}$ compounds, in which the 4f ions display a spin-orbit coupling [26]. Pasatou et al. studied a series of heterodinuclear $\text{Ni}^{\text{II}}\text{-Ln}^{\text{III}}$ Schiff base complexes (Ln^{III} from La^{III} to Er^{III}) and stated that there are antiferromagnetic interactions between Ni^{II} and Ln^{III} ions for Ln^{III} from the beginning of the 4f series (Ce^{III} , Pr^{III} , Nd^{III} , Sm^{III}), while ferromagnetic occurred from Gd^{III} toward the end of the 4f series [26a]. Shiga et al. investigated the magnetic properties of heterotrinuclear $\text{Ni}^{\text{II}}\text{-Ln}^{\text{III}}\text{-Ni}^{\text{II}}$ complexes (Ln^{III} from La^{III} to Lu^{III}) and they indicated that the $\text{Ni}^{\text{II}}\text{-Ln}^{\text{III}}$ interaction is weakly antiferromagnetic for $\text{Ln}^{\text{III}} = \text{Ce}^{\text{III}}$, Pr^{III} and Nd^{III} , and ferromagnetic for $\text{Ln}^{\text{III}} = \text{Gd}^{\text{III}}$, Tb^{III} , Dy^{III} , Ho^{III} and Er^{III} . The $\text{Ni}^{\text{II}}\text{-Ln}^{\text{III}}\text{-Ni}^{\text{II}}$ compounds with diamagnetic La^{III} and Lu^{III} ions showed an antiferromagnetic interaction between the terminal Ni^{II} ions [7a]. Kahn et al.'s magnetic studies of oxamato bridged $\text{Ni}^{\text{II}}\text{-Ln}^{\text{III}}$ compounds also showed that $\text{Ni}^{\text{II}}\text{-Ln}^{\text{III}}$ interaction is antiferromagnetic for $\text{Ln}^{\text{III}} = \text{Ce}^{\text{III}}$, Pr^{III} , Nd^{III} , Er^{III} and ferromagnetic for $\text{Ln}^{\text{III}} = \text{Gd}^{\text{III}}$, Tb^{III} , Dy^{III} and probably Ho^{III} [26c].

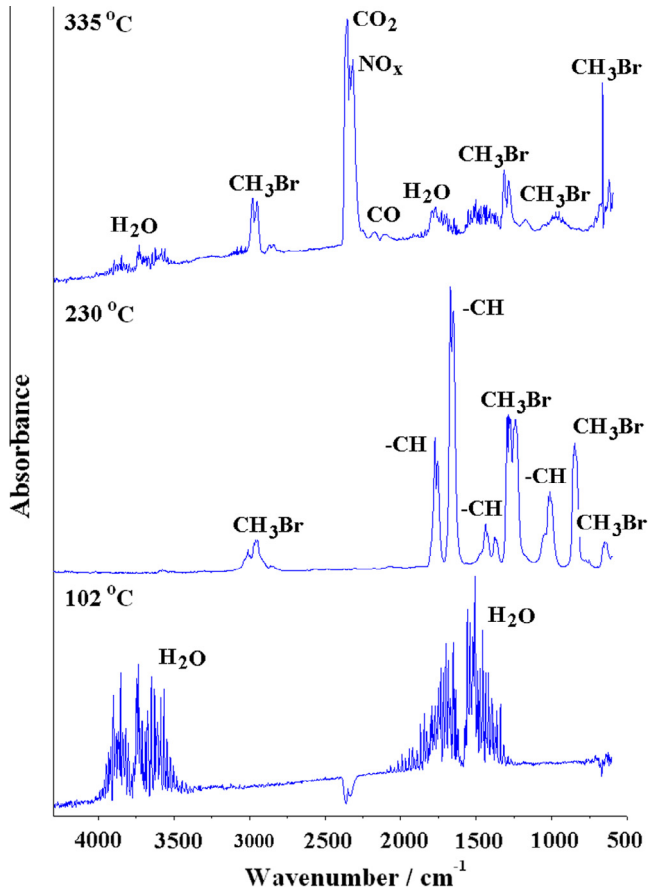


Fig. 6. FTIR spectra of gaseous products of **2** decomposition in argon atmosphere.

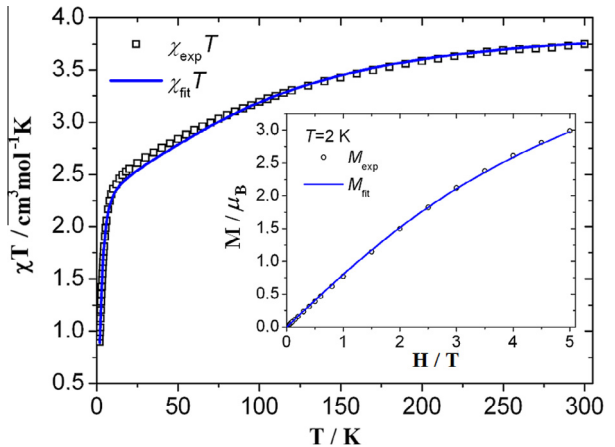


Fig. 8. Temperature dependence of χT for **2**. The inset: Isothermal magnetization at $T = 2$ K.

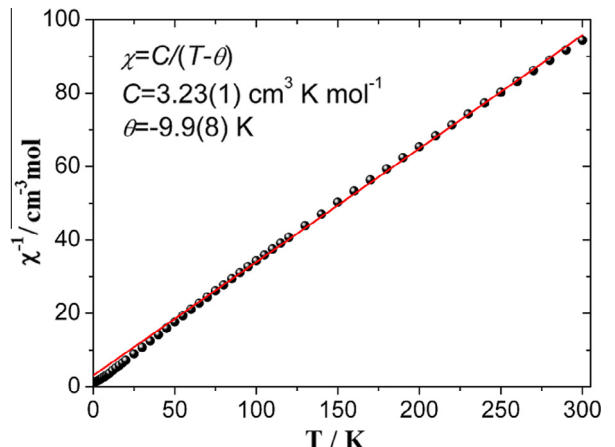


Fig. 9. Temperature dependence of inverse susceptibility of **1**. The red solid line shows the Curie-Weiss fit. (Color online.)

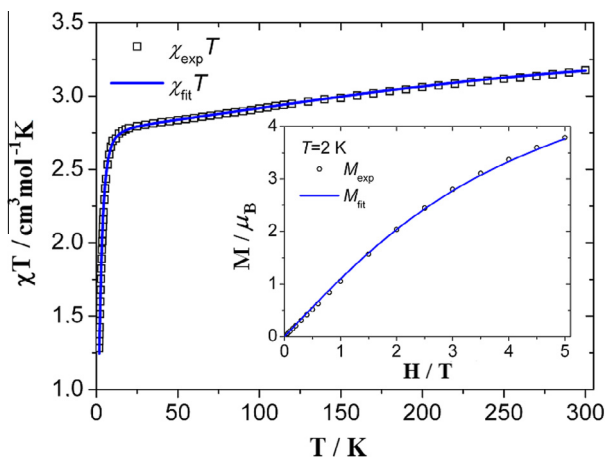


Fig. 7. Temperature dependence of χT for **1**. The inset: Isothermal magnetization at $T = 2$ K.

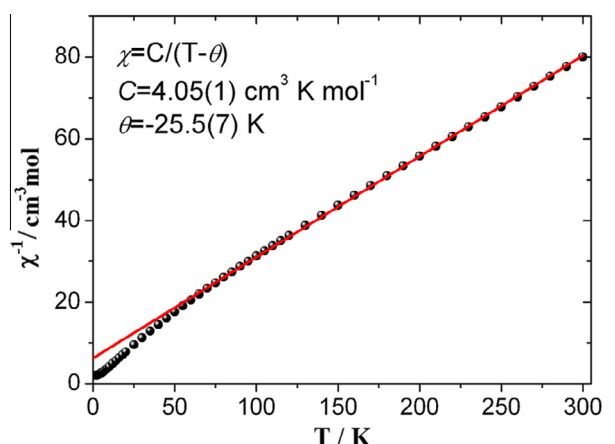


Fig. 10. Temperature dependence of inverse susceptibility of **2**. The red solid line shows the Curie-Weiss fit. (Color online.)

In our compounds the fit of the Curie-Weiss law ($\chi = C/(T - \theta)$) to the inverse molar susceptibility in the temperature range 40–300 K (**1**) and 50–300 K (**2**) yielded $C = 3.23(1) \text{ cm}^3 \text{ K mol}^{-1}$, and $\theta = -9.9(8) \text{ K}$ for **1** (Fig. 9) and $C = 4.05(1) \text{ cm}^3 \text{ K mol}^{-1}$ and $\theta = -25.5(7) \text{ K}$ for **2** (Fig. 10). The negative value of the Weiss constant may indicate the presence of a weak antiferromagnetic intermolecular interaction. Using the value of the Curie constant and assuming the free-ion value of the Landé factor of Ce^{III} ($g_l = 6/7$)/

Pr^{III} ($g_l = 4/5$) and an unknown value of g_{Ni} , one arrives at the estimate $g_{\text{Ni}} \approx 2.20$ (**1**) and $g_{\text{Ni}} \approx 2.21$ (**2**), respectively. In Figs. 7 and 8 the experimental data for the field dependence of the magnetization at $T = 2$ K are shown (open circles). The corresponding curves display a monotonic increase with increasing

value of the magnetic field and reach the value of $3.79 \mu_B$ (in the case of **1**) and $2.99 \mu_B$ (in the case of **2**) at $H = 5$ T. These values are significantly lower than $6.17 \mu_B$ (**1**) and $7.09 \mu_B$ (**2**), respectively expected on the basis of the free-ion approximation calculated at the same values of temperature and external magnetic field. This indicates that the interactions between the Ce^{III}/Pr^{III} and Ni^{II} ions as well as the crystal field effects play a crucial role in defining the magnetic properties of Ni^{II}–Ce^{III}–Ni^{II} (**1**) and Ni^{II}–Pr^{III}–Ni^{II} (**2**) compounds at low temperatures.

3.3.1. Determination of crystal field parameters

The f-electrons in the majority of lanthanide complexes are considered to have properties close to those of isolated ions. The energies of the ground- and excited multiplets are determined by the spin-orbit coupling in which the total angular momentum J is a good quantum number. Fine structure of spectral bands detected in the region from near-IR to UV is ascribed to crystal-field splitting of the ground- and excited multiplets. Many studies devoted to the multiplet structures of lanthanide f systems include only the cases for which sharp emission or absorption bands or both were available [27]. There is yet another approach that can yield some information on the crystal-field splitting, dispenses with the sources of spectroscopic information and uses instead the output of magnetic measurements. Following the ideas of Ishikawa et al.'s [28] we present an approach based solely on magnetic data and use it to estimate the exchange interactions in the studied compounds. A similar approach was already successfully applied in a series of compounds comprising the lanthanide ions [29]. The approach depends crucially on the coordination number (CN) of the lanthanide ion. Crystallographic analysis of isostructural Ni^{II}–Ce^{III}–Ni^{II} (**1**) and Ni^{II}–Pr^{III}–Ni^{II} (**2**) compounds revealed that CN = 10 and the coordination geometry is closest to that of a distorted pentagonal antiprism (PAP, D_{5d}).

The total angular momentum of the ground state in the trivalent cerium/praseodymium ion takes the minimal value, i.e. $J = |L-S|$ (for electronic configuration 4f¹ and 4f², respectively) in the Russell–Saunders coupling scheme, i.e. $J = 5/2$ (for Ce(III)) and $J = 4$ (for Pr(III)). The simulations were carried out using the $2J + 1$ sublevels of the ground-state multiplet of the cerium/praseodymium system. This can be accepted except the complexes containing Eu^{III} and Sm^{III}. For these ions the energy separation between the multiplet of the lowest energy and the first excited multiplet is known to be weak [30]. As a result the low lying excited states may become thermally populated. In addition, the coupling between the substates belonging to different multiplets of the same ground term through the Zeeman perturbation must be also taken into account.

The Hamiltonian pertinent to the present system under external magnetic field is $H_0 = H_Z + H_{CF} + H_{ZFS} + H_E$. The first term accounts for the Zeeman effect. For one Ce^{III}/Pr^{III} ion and two Ni^{II} ions it reads

$$\begin{aligned} H_Z &= \beta(g_{Ce}\mathbf{J} + g_{Ni}\mathbf{S}_{Ni1} + g_{Ni}\mathbf{S}_{Ni2}) \cdot \mathbf{H} \\ H_Z &= \beta(g_{Pr}\mathbf{J} + g_{Ni}\mathbf{S}_{Ni1} + g_{Ni}\mathbf{S}_{Ni2}) \cdot \mathbf{H} \end{aligned}$$

where β is the Bohr magneton and \mathbf{H} denotes the external magnetic field. The total magnetic moment operator $\mu = -\beta(g_{Ce}\mathbf{J} + g_{Ni}\mathbf{S}_{Ni1} + g_{Ni}\mathbf{S}_{Ni2})$ and $\mu = -\beta(g_{Pr}\mathbf{J} + g_{Ni}\mathbf{S}_{Ni1} + g_{Ni}\mathbf{S}_{Ni2})$, respectively is used in the corresponding $|J, J_z\rangle$ representation in its lanthanide part. $\mathbf{S}_{Ni j}$ ($j = 1, 2$) denote the spin one operators of the nickel centers. The spectroscopic tensor of the Ni^{II} centers \mathbf{g}_{Ni} is assumed to be isotropic with its principal value g_{Ni} relaxed during the fitting procedure, whereas the components of $\mathbf{g}_{Ce}/\mathbf{g}_{Pr}$ of which we assume to be diagonal and isotropic were fixed during the fitting procedure. The sec-

ond term corresponds to the crystal field (CF) interaction for the Ce^{III}/Pr^{III} ion, which is expressed in the framework of the extended operator equivalent approach [31–34]. Following the notation by Altshuler and Kozyrev [33], the crystal field part of the Hamiltonian is written as

$$H_{CF} = \sum_{k=2,4,6} \sum_{q=-k}^k B_k^q \mathbf{O}_k^q$$

The coefficients B_k^q are the parameters to be determined. The \mathbf{O}_k^q matrices are polynomials of the total angular momentum matrices $\mathbf{J}^2, \mathbf{J}_z, \mathbf{J}_+, \text{ and } \mathbf{J}_-$ (and their definitions are given in the Table S1). The operator equivalents \mathbf{O}_k^q do not include the operator equivalent coefficients or the radial factors $\langle r^k \rangle$. Both factors are included in the parameters B_k^q , which restricts their application to a single J -manifold. The coefficients are converted into another set of parameters $A_k^q \langle r^k \rangle$ (more commonly used in the literature) using the formula

$$B_k^q = A_k^q \langle r^k \rangle \langle J || \alpha_k || J \rangle$$

where the last factor are the operator-equivalent coefficients. They relate the angular momentum operators to the potential operators and depend on the ion and the coupling scheme assumed (e.g. L–S or intermediate). Their values tabulated for all lanthanide ions in the L–S scheme can be found in [33]. For the 4f¹ electronic configuration (Ce^{III}) the coefficient $\langle J || \alpha_6 || J \rangle$ vanishes, thus only crystal field parameters with $k = 2$ and 4 need be taken into account.

The next component of the Hamiltonian H_{ZFS} includes the zero-field splitting terms for the Ni^{II} ions. It is assumed that the rhombic distortion is negligible. In the local frames of the Ni^{II} ions this contribution reads

$$H_{ZFS} = D_1 \left[\hat{S}_{Ni1z}^2 - 1/3S_{Ni}(S_{Ni} - 1) \right] + D_2 \left[\hat{S}_{Ni2z}^2 - 1/3S_{Ni}(S_{Ni} - 1) \right]$$

Due to the inversion symmetry of the Ni^{II}–Ln^{III}–Ni^{II} (Ln = Ce, Pr) molecule the zero field splitting parameters of both nickel ions are assumed to be equal, i.e. $D_1 = D_2 = D$. The calculations were performed in the local frame of the Ce^{III}/Pr^{III} ion (see the following comments), so the contribution H_{ZFS} had to be duly transformed to that frame.

The last component of the total Hamiltonian H_E is to account for the exchange coupling between the ions. The coupling should be taken between the corresponding spin operators. If we can neglect mixing of the multiplets with different J quantum numbers, so that only the matrix elements within the subspace of wave functions corresponding to the ground term value of J are taken into account, the spin operator \mathbf{S} can be projected onto the total angular momentum operator \mathbf{J} . Equations $\mathbf{L} + \mathbf{S} = \mathbf{J}$ and $\mathbf{L} + 2\mathbf{S} = g\mathbf{J}$ imply that this projection is $\mathbf{S} = (g_J/2)\mathbf{J}$. We further assume that the exchange coupling between the Ni^{II} and Ce^{III}/Pr^{III} ions is isotropic so the Hamiltonian H_E reads

$$\begin{aligned} H_E &= -J_{NiCe}(g_{Ce} - 1)\mathbf{J} \cdot \mathbf{S}_{Ni1} - J_{NiCe}(g_{Ce} - 1)\mathbf{J} \cdot \mathbf{S}_{Ni2} \\ H_E &= -J_{NiPr}(g_{Pr} - 1)\mathbf{J} \cdot \mathbf{S}_{Ni1} - J_{NiPr}(g_{Pr} - 1)\mathbf{J} \cdot \mathbf{S}_{Ni2} \end{aligned}$$

Because the Ni^{II}–Ln^{III}–Ni^{II} (Ln = Ce, Pr) molecule is centrosymmetric we assume a single exchange coupling, identical for both Ni^{II}–Ce^{III}/Pr^{III} pairs.

With an arbitrary choice of a set of B_k^q coefficients and a finite external field, the Hamiltonian H_0 is diagonalized. The determination of a full set of eigenvalues and eigenfunctions permits the calculation of the magnetic molar susceptibility together with the isothermal magnetization. This is performed using the generalized van Vleck formalism

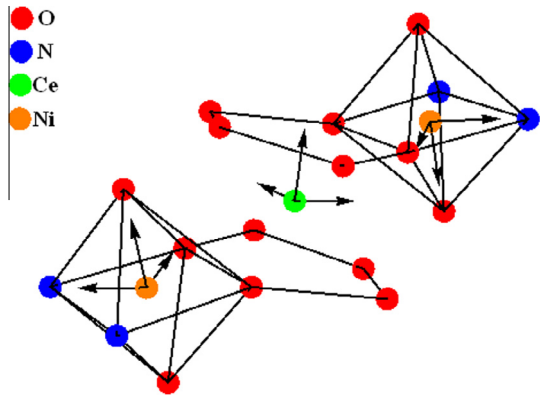


Fig. 11. The main local frame with origin at the Ce^{III} ion and two auxiliary local frames of the Ni^{II} centers.

Table 4

Maximum absorption bands (λ_{max}) and molar absorption coefficients (ε) of the studied compounds.

Compound	λ_{max} [nm]	$(\varepsilon \cdot 10^4 \text{ M}^{-1} \text{ cm}^{-1})$
a free H ₂ L	207.5 (4.42)	236 (4.77)
b Ni ^{II}	204.5 (13.09)	202 (23.00)
c Ni ^{II} -Ln ^{III} -Ni ^{II}	205 (11.44)	240 (13.20)
		283 (2.28)
		359 (1.90)

$$\chi = \frac{N}{3k_B T Z_0} \sum_{n,i} \left[\sum_j \left| \langle \varphi_{n,i} | \mu | \varphi_{n,j} \rangle \right|^2 - 2k_B T \sum_{j,m \neq n} \left| \langle \varphi_{n,i} | \mu | \varphi_{m,j} \rangle \right|^2 \right] \exp\left(-\frac{E_n}{k_B T}\right)$$

$$\mathbf{M} = \frac{N}{Z_H} \sum_k \langle \psi_k | \mu | \psi_k \rangle \exp\left(-\frac{E_k(\mathbf{H})}{k_B T}\right)$$

where $Z_0 = \sum_n d_n \exp(-E_n/k_B T)$, and $Z_H = \sum_k \exp(-E_k(\mathbf{H})/k_B T)$. Here $\varphi_{n,i}$ denote the d_n -fold degenerate eigenfunctions with energy E_n in the absence of magnetic field, whereas the eigensystem $\{\psi_k, E_k(\mathbf{H})\}$ was calculated assuming the nonzero external magnetic field \mathbf{H} . The three principal values of the magnetic susceptibility are denoted

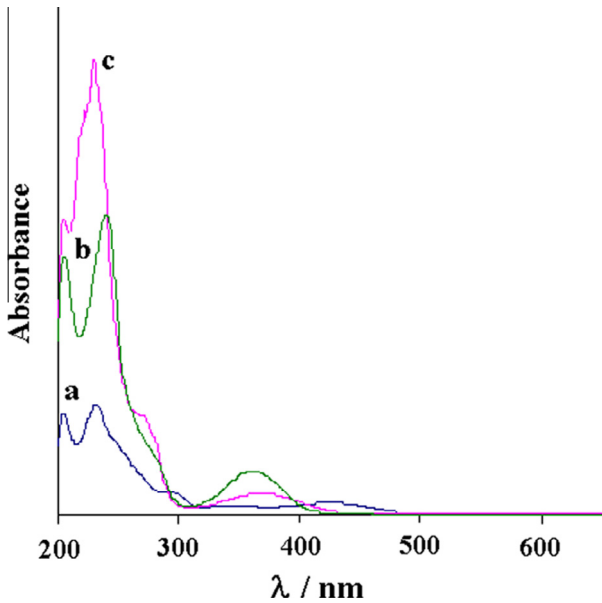


Fig. 12. Electronic absorption spectra of the free ligand H₂L (a), Ni^{II}-Ln^{III}-Ni^{II} (b) and Ni^{II} (c) in methanol at 298 K.

$\chi_{xx}, \chi_{yy}, \chi_{zz}$. The observed molar magnetic susceptibility of powder sample is

$$\bar{\chi} = \frac{1}{3} (\chi_{xx} + \chi_{yy} + \chi_{zz})$$

To calculate the magnetic moment per molecule measured on powder sample one must carry out an appropriate averaging over different orientations of the external magnetic field inducing the moment. For a fixed magnitude H the magnetic field is parametrized with two spherical angles $\mathbf{H}(\theta_i, \phi_j) = H(\sin \theta_i \cos \phi_j, \sin \theta_i \sin \phi_j, -\cos \theta_i)$, where $\theta_i = \arccos [(i-1)/N_\theta]$ ($i = 1, \dots, N_\theta$) and $\phi_j = 2\pi(j-1)/N_\phi$ ($j = 1, \dots, N_\phi$). The calculation is performed for any orientation defined by the pair (θ_i, ϕ_j) and finally the average is calculated as the following mean

$$\bar{M} = \frac{1}{N_\theta N_\phi} \sum_{i=1}^{N_\theta} \sum_{j=1}^{N_\phi} \mathbf{M}(\mathbf{H}) \cdot \mathbf{H}(\theta_i, \phi_j)$$

In the calculations the averaging was carried out over 900 different orientations of the external magnetic field ($N_\theta = 30, N_\phi = 30$).

Fitting was carried out with the help of a specially designed procedure prepared within *Mathematica* 8.0 environment. Two test functions to be minimized were used. The first test function was the relative root-mean-square (r.m.s.) deviation from the measured χT values:

$$\sigma_{\chi T} = \sqrt{\frac{\sum_{i=1}^{N_\chi} [(\bar{\chi}_i T_i)_{\text{theor}} - (\bar{\chi}_i T_i)_{\text{exp}}]^2}{(N_\chi - P) \sum_{i=1}^{N_\chi} (\bar{\chi}_i T_i)_{\text{exp}}^2}},$$

where N_χ denotes the number of experimental points and P the number of free parameters. The other test function one was the relative r.m.s. deviation from the measured M values defined as follows

$$\sigma_M = \sqrt{\frac{\sum_{j=1}^{N_M} [\bar{M}_{j,\text{theor}} - \bar{M}_{j,\text{exp}}]^2}{(N_M - P) \sum_{j=1}^{N_M} \bar{M}_{j,\text{exp}}^2}},$$

where N_M denotes the number of experimental magnetization points. Both test functions were used independently. The fitting procedure was continued until a consistent set of fitted parameters was found. Although the lanthanide site is expected to be of low symmetry (distorted PAP geometry) we assumed initially the

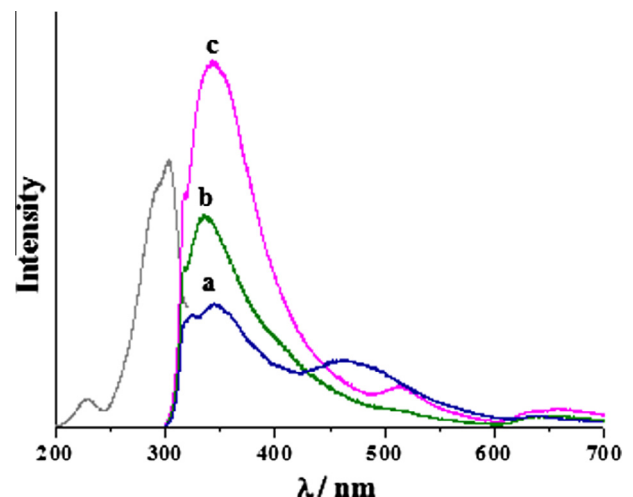


Fig. 13. Excitation (left) spectrum of Ni^{II} (c) ($\lambda_{\text{ob}} = 343 \text{ nm}$) and emission (right) spectra of H₂L (a), Ni^{II}-Ln^{III}-Ni^{II} (b) and Ni^{II} (c) ($\lambda_{\text{ex}} = 292 \text{ nm}$).

crystal field parameter set corresponding to the highest symmetry D_{5d} involving only two nonzero parameters B_2^0 and B_4^0 (in the case of cerium) and four nonzero parameters B_2^0 , B_4^0 , B_6^0 , and B_6^5 (in the case of praseodymium). Otherwise the many-dimensional fits where only powder data are available will be of poor reliability. In the case of compound **2** the simulated susceptibility data revealed a very weak dependence on the crystal field parameter B_6^5 , therefore it was dropped from the calculations. The best fit was obtained successfully with this restricted parameter set. Uncertainties of the parameters were estimated in a standard way using the second derivatives of the test function, which corresponds to the 100% tolerance deviation.

The crystal field parameters B_k^q as well as the zero field splitting tensor do depend on the coordinate frame in which the Hamiltonian is calculated. Therefore one of the first tasks to be done was to fix the local frame in which to do the calculations. Because of the fact that the position of the Ce^{III}/Pr^{III} ion coincides with the inversion center the origin of the local frame was fixed at that position. The coordination sphere of the Ce^{III}/Pr^{III} ion comprises ten oxygen ions denoted in the cif file by symbols O1, O2, O3, O4, and O7 (there are two ions related by inversion symmetry corresponding to one symbol) forming two mutually parallel pentagons. The z axis of the local frame was chosen to point perpendicular to the plane comprising the center of gravity of the pentagonal framework and minimizing the sum of the distances between the plane and the ions. The x direction of the local frame was fixed as the projection onto that plane of the Ni^{II} to Ni^{II} direction. The y axis was determined so that the three axes x, y, and z form a right handed triplet. The coordination sphere of each Ni^{II} ion forming distorted pseudo-octahedral geometry comprises six ions denoted by O1, O2, N1, N2, O6, O8. The z axis of the corresponding local frame was chosen as the direction of the vector joining O8 and O6 ions. The x axis of that frame was assumed to be the direction perpendicular to the z axis and pointing to the position of O1 ion. The y axis was calculated so that the three x, y, and z axes form a right-handed triple. Due to the inversion symmetry the local frames of thus defined local frames of the Ni^{II} ions are related by that symmetry. Fig. 11 shows the main local frame with origin at the Ce^{III} center and both auxiliary local frames of the Ni^{II} centers.

The ground state arising from the 4f¹ configuration of the Ce^{III} ion is $2F_{5/2}$. The dimension of its ground-state subspace is hence 6. The theoretically predicted value of the Landé factor is $6/7 \approx 0.86$. The model system comprises a trinuclear complex Ni^{II}–Ce^{III}–Ni^{II} (**1**) exchange coupled through the oxygen bridges. Due to the inversion symmetry we assume a single exchange coupling constant J_{NiCe} . The best fit to the experimental data was found for the following set of parameters (the CF parameters, the zero-field splitting parameter D, and the exchange coupling are given in cm⁻¹): $g_{\text{Ni}} = 2.23(3)$, $J_{\text{NiCe}} = -1.1(4)$, $D = 6.3(4)$, $A_2^0\langle r^2 \rangle = -265(10)$, $A_4^0\langle r^4 \rangle = 291(6)$. The agreement factors obtained for the susceptibility and magnetization data are 4.2×10^{-5} and 4.4×10^{-4} , respectively. The lowest level is a Kramers doublet built of $|\pm 3/2\rangle$ substates (Table S2). The first excited state comprises the $|\pm 1/2\rangle$ states and the highest Kramers doublet is built of $|\pm 5/2\rangle$ substates. The population of the lowest Kramers doublet at $T = 2$ K is practically 100%. It is only at $T = 150$ K that the population of the first excited level (1.2%) stops being negligible. The populations of the successive Kramers doublets at $T = 200$ K is 95.5%, 3.4%, and 1.1%, respectively. This explains the steady decrease of the χT product on lowering temperature. The sharp down-turn of the χT curve at lowest temperatures is ascribed to the “switching-on” of the positive (spin damping) zero-field splitting of the Ni^{II} centers. Solid lines in Fig. 7 show the best fit curves for the susceptibility and isothermal magnetization.

The ground state arising from the 4f² configuration of the Pr^{III} ion is $3H_4$. The dimension of its ground-state subspace is hence 9. The theoretically predicted value of the Landé factor is $4/5 = 0.8$.

The model system comprises a trinuclear complex Ni^{II}–Pr^{III}–Ni^{II} (**2**) exchange coupled through the oxygen bridges. Due to the inversion symmetry we assume a single exchange coupling constant J_{NiPr} . The best fit to the experimental data was found for the following set of parameters (the CF parameters, the zero-field splitting parameter D, and the exchange coupling are given in cm⁻¹): $g_{\text{Ni}} = 2.15(2)$, $J_{\text{NiPr}} = -1.3(8)$, $D = 7.1(4)$, $A_2^0\langle r^2 \rangle = -310(9)$, $A_4^0\langle r^4 \rangle = 235(11)$, $A_6^0\langle r^6 \rangle = 80(8)$. The agreement factors obtained for the susceptibility and magnetization data are 1.5×10^{-4} and 1.3×10^{-4} , respectively.

The spectrum of the Pr^{III} center consists of one singlet and four doublets. The lowest level is a singlet substate $|0\rangle$ (Table S3). The first excited state comprises the $|\pm 1\rangle$ states and the highest lying doublet is built of $|\pm 2\rangle$ substates. The population of the lowest singlet at $T = 2$ K is practically 100%. It is only at $T = 100$ K that the population of the first excited level (5.9%) stops being negligible. The populations of the successive substates at $T = 150$ K are 81.4%, 16.3%, 1.3%, 0.6%, and 0.4%, respectively. This explains the steady decrease of the χT product on lowering temperature. The sharp down-turn of the χT curve at lowest temperatures is ascribed to the substantial zero-field splitting parameter of the Ni^{II} centers. Solid lines in Fig. 8 show the best fit curves for the susceptibility and isothermal magnetization.

The values of the zero-field splitting parameter $D = 6.3(4)$ cm⁻¹ (**1**) and $D = 7.1(4)$ cm⁻¹ (**2**), respectively are comparable to that found in a trinuclear complex Ni^{II}–Gd^{III}–Ni^{II} [35] ([$(\text{LNi})_2\text{Gd}(\text{NO}_3)_3$, L: triamine1,1,1-tris(aminomethyl)ethane] with octahedral coordination of the nickel ions (4.5 cm⁻¹) [35a]. A lower value (1.5 cm⁻¹) was detected in the heterodinuclear complex [$\text{Ni}^{II}\text{L}\text{Gd}^{III}(\text{hfac})_2(\text{EtOH})$] ($\text{H}_3\text{L} = 1,1,1\text{-tris}[(\text{salicylideneamino})\text{methyl}]$ ethane, hfac = hexafluoroacetylacetone) [35b].

3.4. Electronic absorption spectra and luminescence properties

The photophysical properties of Schiff base ligand H₂L (**a**) and its heterometallic trinuclear Ni^{II}–Pr^{III}–Ni^{II} (**b**) complex have been examined in methanol solution at room temperature and compared with those obtained for mononuclear $[\text{NiL}(\text{H}_2\text{O})_2]$ (**c**) Schiff base complex (the structure of this compound was reported by us earlier [4]). The obtained results are summarized in Table 4 and Figs. 12 and 13. The absorption spectrum of the Schiff base ligand is characterized by three absorption bands in the region 200–600 nm, which are assigned to $\pi-\pi^*$ and $n-\pi^*$ transition, respectively. As shown in Table 4 and Fig. 12, the absorption spectra of the metal complexes exhibit a quite similar absorption profiles. The absorption band maxima of complexes are shifted to lower or higher wavelengths compared to free ligand H₂L, due to complexation. The molar absorption coefficients, ϵ , of both bands of complex Ni^{II}–Pr^{III}–Ni^{II} (**b**) are larger than those of the free ligand H₂L (**a**) and mononuclear Ni(II) complex (**c**). The photoluminescent behavior of all compounds were also studied. The excitation and emission spectra are depicted in Fig. 13. The luminescence spectrum of Schiff base ligand H₂L reveals two of high intensity emission bands at 344 and 465 nm ($\pi^*-\pi$ and π^*-n transitions). The emission spectra of the complexes originate from $\pi-\pi^*$ or ligand-to-metal charge transfer transitions [36]. The emission band maxima of complexes are blue or red shifted compared to free ligand H₂L. Emission maxima appear at 343, 512 and 335 nm respectively for Ni(II) and Ni^{II}–Pr^{III}–Ni^{II} complexes, on UV irradiation ($\lambda_{\text{ex}} = 292$ nm). The emission band at 512 nm of (**c**) can be attributable to the LMCT transition.

Metal cations such as Ni²⁺, Cu²⁺ and Co²⁺ usually quench the organic ligand luminescence [12b,37] in contrast to the Zn²⁺ ion, where the effect is not present [12c,38]. In the case of Ln³⁺ ions an important factor for the effective emission of these ions is energy matching between the Ln³⁺ emitting levels and the ligand

triplet excited state. The absorbed light by the ligands can be transferred to the lanthanide ion by the intramolecular energy transfer. The luminescent properties of the lanthanide metal complexes are strongly dependent on the efficiency of the organic ligand to absorb UV light, the efficiency of energy transfer from the organic ligand to Ln^{3+} ions and the efficiency of Ln^{3+} luminescence [39]. The characteristic luminescence bands of Pr^{3+} did not appear in the heterometallic trinuclear complex (**b**). The reason for this effect is probably the large energy gap between the triplet state level of the H_2L ligand and the emitting level of Pr^{3+} ion. In this conditions energy transfer takes place not efficiently [40]. The Schiff base ligands are good organic ligands to absorb and transfer energy to Sm^{3+} , Eu^{3+} and Tb^{3+} ions. In such systems was observed effectively sensitized luminescence of these ions [12b,40].

In our studies, an enhancement of the emissions, in comparison with the free ligand, was observed in both of Ni^{2+} complexes. It is related to the rigidity of these complexes, which decreases the radiationless deactivation in comparison to the free ligands [38a].

The ligand-based luminescence intensity of mononuclear $\text{Ni}(\text{II})$ compound (**a**) is greater than that of $\text{Ni}^{2+}\text{--Pr}^{3+}\text{--Ni}^{2+}$ (**b**). Therefore, mononuclear $\text{Ni}(\text{II})$ complex has a best emission properties from the studied compounds with low emission quantum yield value of 0.008.

4. Conclusions

The single crystal X-ray analysis of **1** and **2** revealed that they are heterometallic trinuclear $\text{Ni}^{2+}\text{--Ln}^{3+}\text{--Ni}^{2+}$ (where $\text{Ln} = \text{Ce}, \text{Pr}$) coordination compounds with lanthanide ion occupying the center of inversion. The inner salen-type N_2O_2 cavity is occupied by nickel(II), while lanthanide(III) is present in the open and larger O_2O_2 compartment of the dinucleating compartmental ligand. In the crystals **1** and **2** each pair of the $\text{Ni}(\text{II})$ and $\text{Ln}(\text{III})$ metal ions are linked by two bridging phenoxy oxygen atoms of the Schiff base ligand and additionally one acetate ion. The synthesized complexes are stable in air and argon atmosphere at room temperature. Heating of complexes leads at first to the dehydration and next to decomposition processes. The thermal analysis results are in accordance with elemental, FTIR and X-ray analysis. The application of the generalized van Vleck formalism enabled the estimation of the CF parameters for the $\text{Ce}^{3+}/\text{Pr}^{3+}$ ions and the determination of the exchange coupling between the constituent magnetic ions in $\text{Ni}^{2+}\text{--Ln}^{3+}\text{--Ni}^{2+}$ ($\text{Ln} = \text{Ce}, \text{Pr}$) compounds. The best fit was obtained with the assumption of the highest symmetry of the coordination geometry involving only two CF parameters $A_2^0(r^2)$ and $A_4^0(r^4)$ (for **1**) and three CF parameters $A_2^0(r^2)$, $A_4^0(r^4)$, and $A_6^0(r^6)$ (for **2**). For $\text{Ni}^{2+}\text{--Ce}^{3+}\text{--Ni}^{2+}$ (**1**) the exchange coupling mediated through the oxygen atoms was found to be rather weak and antiferromagnetic ($J_{\text{NiCe}} = -1.1(4) \text{ cm}^{-1}$). In the case of $\text{Ni}^{2+}\text{--Pr}^{3+}\text{--Ni}^{2+}$ (**2**) this value ($J_{\text{NiPr}} = -1.3(8) \text{ cm}^{-1}$) is quite large for 3d–4f system and also confirms the antiferromagnetic interaction between Pr^{3+} and Ni^{2+} ions. The values of the zero-field splitting parameter D obtained for **1** and **2** are equal $6.3(4)$ and $7.1(4) \text{ cm}^{-1}$ respectively. The substantial value of the Weiss constant for compound **2** should be attributed to the presence of the crystal field and zero-field splitting, rather than to the presence of an antiferromagnetic intermolecular interaction. The ligand-based luminescence intensity of $\text{Ni}^{2+}\text{--Pr}^{3+}\text{--Ni}^{2+}$ is less than that of mononuclear $\text{Ni}(\text{II})$ complex.

Appendix A. Supplementary data

CCDC 931236 and 931236 contains the supplementary crystallographic data for **1** and **2**. These data can be obtained free of charge via <http://www.ccdc.cam.ac.uk/conts/retrieving.html>, or from the Cambridge Crystallographic Data Centre, 12 Union Road,

Cambridge CB2 1EZ, UK; fax: (+44) 1223 336 033; or e-mail: deposit@ccdc.cam.ac.uk. Supplementary data associated with this article can be found, in the online version, at <http://dx.doi.org/10.1016/j.poly.2013.10.019>.

References

- [1] (a) A. Bhunia, M. Yadav, Y. Lan, A.K. Powell, F. Menges, C. Riehn, G. Niedner-Schäferburg, P.P. Jana, R. Riedel, K. Harms, S. Dehnend, P.W. Roesky, Dalton Trans. 42 (2013) 2445;
 (b) G. Peng, L. Ma, L. Liang, Y. Ma, C. Yang, H. Deng, Cryst. Eng. Commun. 15 (2013) 922;
 (c) Y. Sun, S. Wang, K. Li, E.-J. Gao, G. Xiong, M. Guo, Inorg. Chem. Commun. 28 (2013) 1;
 (d) S. Hino, M. Maeda, K. Yamashita, Y. Kataoka, M. Nakano, T. Yamamura, H. Nojiri, M. Kotu, O. Yamamurod, T. Kajiwara, Dalton Trans. 42 (2013) 2683;
 (e) M.-X. Yao, Q. Zheng, K. Qian, Y. Song, S. Gao, J.-L. Zuo, Chem. Eur. J. 19 (2013) 294.
- [2] (a) D. Zou, W. Feng, G. Shi, X. Lü, Z. Zhang, Y. Zhang, H. Liu, D. Fan, W.-K. Wong, R.A. Jones, Spectrochim. Acta, Part A 9835 (2012) 9;
 (b) W.-Y. Bi, X.-Q. Lü, W.-L. Chai, T. Wei, J.-R. Song, S.-S. Zhao, W.-K. Wong, Inorg. Chem. Commun. 12 (2009) 267;
 (c) X.-Q. Lü, W.-X. Feng, Eur. J. Inorg. Chem. (2010) 2714;
 (d) X.-P. Yang, D. Schipper, A. Liao, J.M. Stanley, R.A. Jones, B.J. Holliday, Polyhedron 52 (2012) 165.
- [3] X.-P. Yang, R.A. Jones, W.-K. Wong, V. Lynch, M.M. Oye, A.L. Holmes, Chem. Commun. (2006) 1836.
- [4] (a) B. Cristóvão, J. Klak, B. Miroslaw, L. Mazur, Inorg. Chim. Acta 378 (2011) 288;
 (b) B. Cristóvão, B. Miroslaw, J. Klak, Polyhedron 34 (1) (2012) 121;
 (c) B. Cristóvão, J. Klak, B. Miroslaw, Polyhedron 43 (1) (2012) 247.
- [5] (a) M. Andruh, J.P. Costes, C. Diaz, S. Gao, Inorg. Chem. 48 (2009) 3342;
 (b) R. Koner, H.H. Lin, H.H. Wei, S. Mohanta, Inorg. Chem. 44 (2005) 3524;
 (c) R. Watanabe, K. Fujiwara, A. Okazawa, G. Tanaka, S. Yoshii, H. Nojiri, T. Ishida, Chem. Commun. 47 (2011) 2110;
 (d) A. Okazawa, R. Watanabe, M. Nezu, T. Shimada, S. Yoshii, H. Nojiri, T. Ishida, Chem. Lett. 39 (2010) 1331.
- [6] (a) J.P. Costes, S. Shova, W. Wernsdorfer, Dalton Trans. (2008) 1843;
 (b) J.P. Costes, L. Vendier, Eur. J. Inorg. Chem. (2010) 2768;
 (c) J.P. Costes, F. Dahan, A. Dupuis, J.P. Laurent, Inorg. Chem. 35 (1996) 2400;
 (d) J.P. Costes, F. Dahan, C.R. Acad.Sci. Paris Chim. Chem. 4 (2001) 97;
 (e) J.P. Costes, F. Dahan, A. Dupuis, Inorg. Chem. 39 (2000) 165;
 (f) J.P. Costes, F. Dahan, A. Dupuis, Inorg. Chem. 39 (2000) 5994;
 (g) J.P. Costes, F. Dahan, A. Dupuis, J.P. Laurent, Chem. Eur. J. 4 (1998) 1616.
- [7] (a) T. Shiga, N. Ito, A. Hidaka, H. Ohkawa, S. Kitagawa, M. Ohba, Inorg. Chem. 46 (2007) 3492;
 (b) T.D. Pasatouli, J.P. Sutter, A.M. Madalan, F.Z. Chiboub Fellah, C. Duhayon, M. Andruh, Inorg. Chem. 50 (2011) 5890;
 (c) V. Chandrasekhar, B.M. Pandian, R. Boomishankar, A. Steiner, J.J. Vittal, A. Hour, Inorg. Chem. 47 (2008) 4918;
 (d) Z. Xu, P.W. Read, D.E. Hibbs, M.B. Hursthous, K.M.A. Malik, Inorg. Chem. 39 (2000) 508;
 (e) S.R. Bayly, Z. Xu, B.O. Patrick, S.J. Rettig, M. Pink, R.C. Thompson, C. Orvig, Inorg. Chem. 42 (2003) 1576.
- [8] (a) M.L. Kahn, P. Lecante, M. Verelst, C. Mathoniere, O. Kahn, Chem. Mater. 12 (2000) 3073;
 (b) S. Igarashi, S. Kawaguchi, Y. Yukawa, F. Tuna, R.E.P. Winpenny, Dalton Trans. (2009) 3140;
 (c) A.N. Georgopoulou, R. Adam, C.P. Raptopoulou, V. Psycharis, R. Ballesteros, B. Abarca, K. Boudalis, Dalton Trans. 39 (2010) 5020.
- [9] (a) E. Colacio, J. Ruiz-Sánchez, F.J. White, E.K. Brechin, Inorg. Chem. 50 (2011) 7268;
 (b) C. Papatriantafyllopoulou, M. Estrader, C.G. Efthymiou, D. Dermitzaki, K. Gkotsis, A. Terzis, C. Diaz, S.P. Perlepes, Polyhedron 28 (2009) 1652;
 (c) A.N. Georgopoulou, C.G. Efthymiou, C. Papatriantafyllopoulou, Polyhedron 30 (2011) 2978;
 (d) M. Sakamoto, K. Manseki, H. Ōkawa, Coord. Chem. Rev. 219–221 (2001) 379.
- [10] (a) A.M. Atria, Y. Moreno, E. Spodine, M.T. Garland, R. Baggio, Inorg. Chim. Acta 335 (2002) 1;
 (b) T.D. Pasatouli, M. Etienne, A.M. Madalan, M. Andruh, R. Sessoli, Dalton Trans. 39 (2010) 4802;
 (c) C.G. Efthymiou, T.C. Stamatatos, C. Papatriantafyllopoulou, A.J. Tasiopoulos, W. Wernsdorfer, S.P. Perlepes, G. Christou, Inorg. Chem. 49 (2010) 9737;
 (d) C.G. Efthymiou, A.N. Georgopoulou, C. Papatriantafyllopoulou, A. Terzis, C.P. Raptopoulou, A. Escuer, S.P. Perlepes, Dalton Trans. 39 (2010) 8603;
 (e) K.C. Mondal, G.E. Kostakis, Y. Lan, W. Wernsdorfer, C.E. Anson, A.K. Powell, Inorg. Chem. 50 (2011) 11604.
- [11] (a) R. Koner, G.H. Lee, Y. Wang, H.H. Wei, S. Mohanta, Eur. J. Inorg. Chem. (2005) 1500;
 (b) J.H. Wang, P.F. Yan, G.M. Li, J.W. Zhang, P. Chen, M. Suda, Y. Einaga, Inorg. Chim. Acta 363 (2010) 3706.
- [12] (a) S. Liao, X.-P. Yang, R.A. Jones, Cryst. Growth Des. 12 (2012) 970;
 (b) X.-P. Yang, D. Lam, C. Chan, J.M. Stanley, R.A. Jones, B.J. Holliday, W.-K.

- Wong, Dalton Trans. 40 (2011) 9795;
- (c) W.-K. Lo, W.-K. Wong, W.-Y. Wong, J. Guo, K.-T. Yeung, Y.-K. Cheng, X.-P. Yang, R.A. Jones, Inorg. Chem. 45 (2006) 9315;
- (d) W.-K. Wong, X.-P. Yang, R.A. Jones, J.H. Rivers, V. Lynch, W.-K. Lo, D. Xiao, M.M. Oye, A.L. Holmes, Inorg. Chem. 45 (2006) 4340;
- (e) X.-P. Yang, R.A. Jones, J. Am. Chem. Soc. 127 (2005) 7686;
- (f) X.-P. Yang, R.A. Jones, V. Lynch, M.M. Oye, L.H. Archie, Dalton Trans. (2005) 849;
- (g) X.-P. Yang, R.A. Jones, J.H. Rivers, W.-K. Wong, Dalton Trans. (2009) 10505;
- (h) X.-P. Yang, C. Chan, D. Lam, D. Schipper, J.M. Stanley, X. Chen, R.A. Jones, B.J. Holliday, W.-K. Wong, S. Chena, Q. Chen, Dalton Trans. 41 (2012) 11449.
- [13] S. Zhao, X. Lü, A. Hou, W.-Y. Wong, W.-K. Wong, X. Yang, R.A. Jones, Dalton Trans. (2009) 9595.
- [14] X. Lü, W. Bi, W. Chai, J. Song, J. Meng, W.-Y. Wong, W.-K. Wong, X. Yang, R.A. Jones, Polyhedron 28 (2009) 27.
- [15] (a) X.-P. Yang, R.A. Jones, W.-K. Wong, Chem. Commun. (2008) 3266;
- (b) X.-P. Yang, R.A. Jones, W.-K. Wong, Dalton Trans. (2008) 1676;
- (c) W.-Y. Bi, X.-Q. Lü, Z. Anorg. Allg. Chem. 634 (2008) 1795;
- (d) X.-P. Yang, B.P. Hahn, R.A. Jones, W.-K. Wong, K.J. Stevenson, Inorg. Chem. 46 (2007) 7050;
- (e) X.-P. Yang, R.A. Jones, M.M. Oye, A.L. Holmes, W.-K. Wong, Cryst. Growth Des. 6 (2006) 2122;
- (f) X.-P. Yang, R.A. Jones, Q. Wu, M.M. Oye, W.-K. Lo, W.-K. Wong, A.L. Holmes, Polyhedron 25 (2006) 271.
- [16] G.A. Bain, J.F. Berry, J. Chem. Educ. 85 (2008) 532.
- [17] W.R. Dawson, M.W. Windsor, J. Phys. Chem. 72 (1968) 3251.
- [18] J.N. Demas, G.A. Crosby, J. Phys. Chem. 75 (1971) 991.
- [19] Oxford Diffraction, Xcalibur CCD System, CRYSTALIS Software System, version 1.171, Oxford Diffraction Ltd., 2009.
- [20] R.C. Clark, J.S. Reid, Acta Crystallogr., Sect. A 51 (1995) 887.
- [21] G.M. Sheldrick, Acta Crystallogr., Sect. A 64 (2008) 112.
- [22] ORTEP3 for Windows L.J. Farrugia, J. Appl. Crystallogr. 30 (1997) 565.
- [23] Diamond – Crystal and Molecular Structure Visualization – Crystal Impact – K. Brandenburg & H. Putz GbR, Rathausgasse 30, D-53111.
- [24] (a) A.A.A. Aziz, A.N.M. Salem, M.A. Sayed, M.M. Aboaly, J. Mol. Struct. 1010 (2012) 130;
- (b) S.O. Bahaffi, A.A.A. Aziz, M.M. El-Naggar, J. Mol. Struct. 1020 (2012) 188;
- (c) T. Rosu, E. Pahontu, C. Maxim, R. Georgescu, N. Stanica, A. Gulea, Polyhedron 30 (2011) 154.
- [25] (a) X. Jiang, C. Li, Y. Chi, J. Yan, J. Hazard. Mater. 173 (2010) 205;
- (b) T. Xu, X. Huang, Fuel 89 (2010) 2185;
- (c) M. Sun, X.-X. Ma, Q.-X. Yao, R.-C. Wang, Y.-X. Ma, G. Feng, J.-X. Shang, L. Xu, Y.-H. Yang, Energy Fuels 25 (2011) 1140;
- (d) L. Tao, G.-B. Zhao, J. Qian, Y.-K. Qin, J. Hazard. Mater. 175 (2010) 754;
- (e) X. Jiang, C. Li, T. Wang, B. Liu, Y. Chi, J. Yan, J. Anal. Appl. Pyrolysis 84 (2009) 103.
- [26] (a) T.D. Pasatouji, J.P. Sutter, A.M. Madalan, F.Z. Chiboub, Fellah, C. Duhayon, M. Andruh, Inorg. Chem. 50 (2011) 5890;
- (b) M.L. Kahn, P. Lecante, M. Verelst, C. Mathonie're, O. Kahn, Chem. Mater. 12 (2000) 3073.
- [27] (a) J. Cybińska, J. Hölsä, M. Lastusaari, J. Legendziewicz, G. Meyer, C. Wickleder, J. Alloys Compd. 380 (2004) 27;
- (b) E. Gałdecka, Z. Gałdecki, J. Cybińska, R.J. Wiglus, V. Amirkhanov, J. Legendziewicz, J. Mol. Phys. 101 (2003) 1015;
- (c) M.N. Popova, S.A. Klimin, E.P. Chukalina, B.Z. Malkin, R.Z. Levitin, B.V. Mill, E. Antic-Fidancev, Phys. Rev. B 68 (2003) 155103;
- (d) G. Oczko, J. Legendziewicz, M.S. Wickleder, G. Meyer, J. Alloys Compd. 341 (2002) 255;
- (e) J. Cybińska, J. Sokolnicki, J. Legendziewicz, G. Meyer, J. Alloys Compd. 341 (2002) 115;
- (f) O.L. Malta, J. Legendziewicz, E. Huskowska, I. Turowska-Tyrk, R.Q. Albuquerque, C. de Mello Donegá, F.R.G. de Silva, J. Alloys Compd. 323–324 (2001) 654;
- (g) J. Legendziewicz, M. Borzechowska, G. Oczko, G. Meyer, New J. Chem. 24 (2000) 53;
- (h) J. Legendziewicz, M. Borzechowska, G. Oczko, J. Mroziński, Spectrochim. Acta, Part A 54 (1998) 2197.
- [28] (a) N. Ishikawa, M. Sugita, T. Okubo, N. Tanaka, T. Iino, Y. Kaizu, Inorg. Chem. 42 (2003) 2440;
- (b) N. Ishikawa, T. Iino, Y. Kaizu, J. Phys. Chem. A 106 (2002) 9543;
- (c) N. Ishikawa, I. Tino, Y. Kaizu, J. Am. Chem. Soc. 124 (2002) 11440.
- [29] P. Przychodzeń, R. Pełka, K. Lewiński, J. Supel, M. Rams, K. Tomala, B. Sieklucka, Inorg. Chem. 46 (2007) 8924.
- [30] M. Kozięć, R. Pełka, M. Rams, W. Nitek, B. Sieklucka, Inorg. Chem. 49 (2010) 4268.
- [31] K.W.H. Stevens, Proc. Phys. Soc., London, Sect. A 65 (1952) 209.
- [32] A. Abragam, B. Bleaney, Electron Paramagnetic Resonance of Transition Ions, Clarendon Press, Oxford, 1970.
- [33] S. Altshuler, B.M. Kozyrev, Electron Paramagnetic Resonance in Compounds of Transition Elements, Nauka, Moscow, 1972 (in Russian).
- [34] O. Kahn, Molecular Magnetism, VCH, New York, 1993.
- [35] (a) J.P. Costes, T. Yamaguchi, M. Kojima, L. Vendier, Inorg. Chem. 48 (2009) 5555;
- (b) T. Yamaguchi, Y. Sunatsuki, H. Ishida, M. Kojima, H. Akashi, Inorg. Chem. 47 (2008) 5736.
- [36] (a) B. Tao, F. Cheng, X. Jiang, H. Xia, J. Mol. Struct. 1028 (2012) 176;
- (b) J. Yang, Q. Yue, G.D. Li, J.J. Cao, G.H. Li, J.S. Chen, Inorg. Chem. 45 (2006) 2857;
- (c) Y. Cui, Y. Yue, G. Qian, B. Chen, Chem. Rev. 112 (2012) 1126;
- (d) C.R. Bhattacharjee, G. Das, P. Mondal, Eur. J. Inorg. Chem. (2011) 5390;
- (e) J.M. Lin, W.B. Chen, X.M. Lin, A.H. Lin, C.Y. Ma, W. Dong, C.-E. Tian, Chem. Commun. 47 (2011) 2402.
- [37] (a) S.B. Jiménez-Pulido, F.M. Linares-Ordóñez, M.N. Moreno-Carretero, Polyhedron 28 (2009) 2641;
- (b) S.A. Patil, S.N. Unki, A.D. Kulkarni, V.H. Naik, P.S. Badami, Spectrochim. Acta, Part A 79 (2011) 1128;
- (c) Q.H. Wang, W. Weng, J.M. Liu, L.Z. Cai, G.C. Guo, J. Coord. Chem. 59 (2006) 485;
- (d) K. Singh, Y. Kumar, P. Puri, G. Singh, Bioinorg. Chem. Appl. doi:10.1155/2012/729708.;
- (e) B. Pedras, L. Fernandes, E. Oliveira, L. Rodríguez, M.M.M. Raposo, J.L. Capelo, C. Lodeiro, Inorg. Chem. Commun. 12 (2009) 79;
- (f) M. Barwiolek, E. Szlyk, T.M. Muziol, T. Lis, Dalton Trans. 40 (2011) 11012.
- [38] (a) J. Rojo, F.J. Romero-Salguero, J.-M. Lehn, G. Baum, D. Fenske, Eur. J. Inorg. Chem. (1999) 1421;
- (b) A.R. Stefankiewicz, M. Wałęsa, P. Jankowski, A. Ciesielski, V. Patroniak, M. Kubicki, Z. Hnatejko, J.M. Harrowfield, J.-M. Lehn, Eur. J. Inorg. Chem. (2008) 2910;
- (c) T. Wei, S. Zhao, W. Bi, X. Lü, Y. Hui, J. Song, W.-K. Wong, R.A. Jones, Inorg. Chem. Commun. 12 (2009) 1216.
- [39] (a) W.T. Carnall, in: K.A. Gschneidner, L.R. Eyring (Eds.), Handbook on the Physical and Chemistry of Rare Earths, vol. 3, North Holland, Amsterdam, 1979.;
- (b) J.-C.G. Bunzli, in: J.-C.G. Bunzli, G.R. Choppin (Eds.), Lanthanide Probes in Life, Chemical and Earth Sciences, Elsevier, Amsterdam, 1989.;
- (c) S. Lis, M. Elbanowski, B. Mąkowska, Z. Hnatejko, J. Photochem. Photobiol. A: Chem. 150 (2002) 233.
- [40] (a) Z.A. Taha, A.M. Ajlouni, W. Al Momani, J. Lumin. 132 (2012) 2832;
- (b) A. Listkowski, W. Osińska, J. Mohanraj, M. Pietraszkiewicz, G. Dutkiewicz, T. Borowiak, Synth. Met. 162 (2012) 1285;
- (c) P. Gawryszewska, J. Lisowski, Inorg. Chim. Acta 383 (2012) 220.